Comprehensive properties assessment of asphalt binder under aqueous solutions with different pH values and its gradient damage behaviors

Zou, Yingxue; Wu, Shaopeng; Chen, Anqi; Liu, Quantao; Amirkhanian, Serji; Xu, Shi; Yang, Chao; Wan, Pei; Xu, Haiqin; Lu, Ziyu

DOI
10.1016/j.conbuildmat.2024.134938

Publication date
2024

Document Version
Final published version

Published in
Construction and Building Materials

Citation (APA)
Zou, Y., Wu, S., Chen, A., Liu, Q., Amirkhanian, S., Xu, S., Yang, C., Wan, P., Xu, H., & Lu, Z. (2024). Comprehensive properties assessment of asphalt binder under aqueous solutions with different pH values and its gradient damage behaviors. *Construction and Building Materials*, *414*, Article 134938. https://doi.org/10.1016/j.conbuildmat.2024.134938

Construction and Building Materials 414 (2024) 134938

Contents lists available at ScienceDirect

Construction and Building Materials

journal homepage: www.elsevier.com/locate/conbuildmat

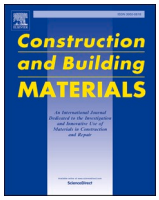

Comprehensive properties assessment of asphalt binder under aqueous solutions with different pH values and its gradient damage behaviors

Yingxue Zou [a], Shaopeng Wu [a,*], Anqi Chen [a], Quantao Liu [a], Serji Amirkhanian [b], Shi Xu [c,d], Chao Yang [e], Pei Wan [a], Haiqin Xu [a], Ziyu Lu [f]

[a] State Key Laboratory of Silicate Materials for Architectures, Wuhan University of Technology, Luoshi Road 122, Wuhan 430070, China
[b] Department of Civil Construction and Environmental Engineering, University of Alabama, Tuscaloosa, AL 35487, USA
[c] School of Civil Engineering and Architecture, Wuhan University of Technology, Luoshi Road 122, Wuhan 430070, China
[d] Faculty of Civil Engineering and Geosciences, Delft University of Technology, Stevinweg 1, 2628 CN Delft, the Netherlands
[e] School of Civil Engineering, Architecture and Environment, Hubei University of Technology, Wuhan 430068, China
[f] School of Transportation and Logistics Engineering, Wuhan University of Technology, Wuhan 430063, China

ARTICLE INFO

Keywords:
Asphalt binder
pH value
Aqueous solutions
Comprehensive assessment
Gradient damage behaviors

ABSTRACT

This study characterized the morphology, high-temperature property, rheological property, adhesion, cohesion, and chemical component of asphalt binder under aqueous solutions of different pH values. Then the physico-chemical properties of asphalt binder were comprehensively evaluated by the improved radar chart. The properties of asphalt binder stripped layer-by-layer were explored to elucidate its gradient damage behaviors. The results indicate that the pH 3 solution reveals the greatest impact on the morphology of 90 asphalt (90 A) and styrene-butadiene-styrene modified asphalt (SBS MA), leading to the wide cracks on 90 A and the network cracks on SBS MA. The comprehensive assessment index of 90 A exposed to pH 3, pH 5, pH 7, pH 9, and pH 11 solutions can be reduced by 20.8%, 20.2%, 1.5%, 14.0%, and 25.5%, respectively. While for SBS MA, its corresponding values variation are 23.2%, 17.7%, 4.6%, 8.7%, and 13.0%, respectively. The acid solutions significantly affect the comprehensive properties of 90 A, but their pH value has little effect. 90 A exposure to the higher pH value of alkali solution reveals the worse comprehensive properties. Acid solute and alkali solute can aggravate the effect of aqueous solution on the comprehensive properties of SBS MA, and the degree of aggravation increases with the increase of solute concentration. The properties of asphalt binders exhibit varied gradient damage behaviors under different solute environments. The most serious damage occurs at 25–50 μm of 90 A and 0–50 μm of SBS MA. This study facilitates an accurate understanding of the mechanism of pavement distresses and composition design and construction utilization of asphalt binders.

1. Introduction

Asphalt binder is a complex mixture of heavy hydrocarbons of various structures, mixing aliphatic, naphthenic, and aromatic hydrocarbons [1]. As a binder, it binds aggregates, fillers, and other materials closely together. After uniform mixing, it is used in pavement engineering. Asphalt pavement has advantages such as high ride comfort, low noise, good crack resistance, and convenient construction, so it is widely applied on municipal roads, highways, airport runways, etc [2,3]. However, during service, it is prone to distress like stripping, slurry, potholes, and cracking due to exposure to external environments such as rainwater and groundwater [4–6]. This can seriously affect driving safety and the economic costs of asphalt pavement [7–9]. Therefore, the in-depth study of moisture damage on asphalt pavement has important guiding significance for improving pavement durability.

With the rapid development of modern industry, industrial pollution has become the most urgent problem facing mankind. The gas emissions generated by the enormous chemical industry chain contain rich sulfur dioxide and nitrogen oxides, which combine with atmospheric water vapor to form acid rain with a pH of less than 3 [10,11]. The area of alkali soil in China is about 36 million hectares, mainly distributed in Northeast China and the Huang-Huai-Hai region [12]. The groundwater in these areas is high in mineral substances, with a pH value generally between 8.5–10 [13]. Deserts cover about one-third of the Earth's land

* Corresponding author.
E-mail address: wusp@whut.edu.cn (S. Wu).

https://doi.org/10.1016/j.conbuildmat.2024.134938
Received 14 October 2023; Received in revised form 5 December 2023; Accepted 5 January 2024
Available online 17 January 2024

area [14]. The desert area in China is about 3.3 million square kilometers, mainly distributed in Xinjiang, Inner Mongolia, Gansu, and other provinces [15]. The groundwater pH near Dunhuang, Gansu can reach above 11, which is strongly alkaline [16]. The groundwater in deserts and alkali soils is moderate to strongly alkaline, and can easily infiltrate into roadbeds through capillary action. As an important environmental parameter, the pH value of the aqueous solution will have a certain effect on the physical and chemical properties of the asphalt binder, causing erosion to asphalt pavement.

Asphalt binder is the binder in the mixture, and its physicochemical properties directly determine the road performance of asphalt mixtures and play a decisive role in the life of asphalt pavement [51]. For the conventional performance indicators, some studies have shown that acid and alkali solutions can reduce the softening point and viscosity of asphalt binder, increase the degree of penetration, and reduce the thermal stability, and the negative effect of acid solution is more significant [17]. In terms of dynamic viscosity, the acid solution reduces the composite viscosity of asphalt, while the alkali solution has less effect. With regard to aging properties, the aging resistance of asphalt can be significantly reduced by acid and alkali solutions [18]. For the characteristics of asphalt components, it can be found that acid solutions result in a relative increase in aromatic hydrocarbons, while alkali solutions cause an increase in the content of saturated hydrocarbons [19]. As far as the microstructure and morphology of asphalt are concerned, both acid and alkali solutions can destroy its internal structure and loosen the asphalt mesh structure [20]. Acid solutions can corrode the asphalt film, creating more cracks and holes. Alkaline solutions promote blistering of the asphalt surface. In terms of the interfacial bond between asphalt binder and aggregate, both acid and alkali solutions can reduce the interfacial bond strength. Acid solutions are more likely to destroy the cohesion, while alkali solutions affect the adhesion [18]. The effects of acid and alkali solutions on asphalt-based materials should not be underestimated, thus the decay mechanism of asphalt binder under different pH solutions has been gradually explored by scholars. Asphalt contains several water-sensitive components (e.g. carboxylic acids, sulphonic acids, fatty amines, amides, esters, aliphatics, etc.), which can interact with aqueous solutions [21]. The acid solution leads to oxidation, stabilization, and polymerization of asphalt binder, resulting in significant changes in asphalt properties [17]. The alkali solute inhibits the diffusion of water molecules and promotes the formation of hydrogen bonds on the aggregate surface. Alkali solution is the most destructive to the asphalt solution-aggregate interface [22]. In summary, the research on the effect of acid and alkali aqueous solutions on asphalt performance has made some progress. However, the influence of acid and alkali solution on the physicochemical properties of asphalt binder has not been unified, and the influence of pH value has not been comprehensively assessed [23]. Additionally, short-term exposure to aqueous solutions leads to an increase in the elastic component and stiffness of the asphalt binder, a decrease in the fatigue life of the asphalt binder, and a decrease in the cohesion and adhesion to the aggregate [18]. Long-term exposure to the aqueous solution leads to a reduction in the polar component of the asphalt binder, an increase in the viscous component, and a further reduction in the cohesion and adhesion to the aggregate [24]. Exposure time has a significant impact on the change of asphalt properties, and the deeper evolutionary mechanism regarding the effect of acid and alkaline solution treatments on asphalt properties remains to be further elucidated.

Therefore, considering the exposure time and the depth of the asphalt layer, the research on the influence law of aqueous solution pH on asphalt performance was carried out in this study. The research scheme is shown in Fig. 1, the indoor simulation test methods, including digital measurement (DM), softening point (SP) test, dynamic shear rheometer (DSR) test, pull-out (PO) test, and Fourier transform infrared spectroscopy (FTIR) test, were adopted to comprehensively assess the influence law of acid and alkaline environments on the performance of asphalt binder and its gradient damage behaviors. It can provide a theoretical basis for understanding the mechanism of pavement distresses and for the design, construction, and use of asphalt binders.

2. Materials and experiments

2.1. Materials

The asphalt binders used in this study were base 90 asphalt (90 A) binder with performance grade 70–22, and styrene-butadiene-styrene modified asphalt (SBS MA) binder with performance grade 70–28. Both were obtained from Inner Mongolia Xindalu Asphalt Co., Ltd (Inner Mongolia, China). Due to their stable properties and wide availability,

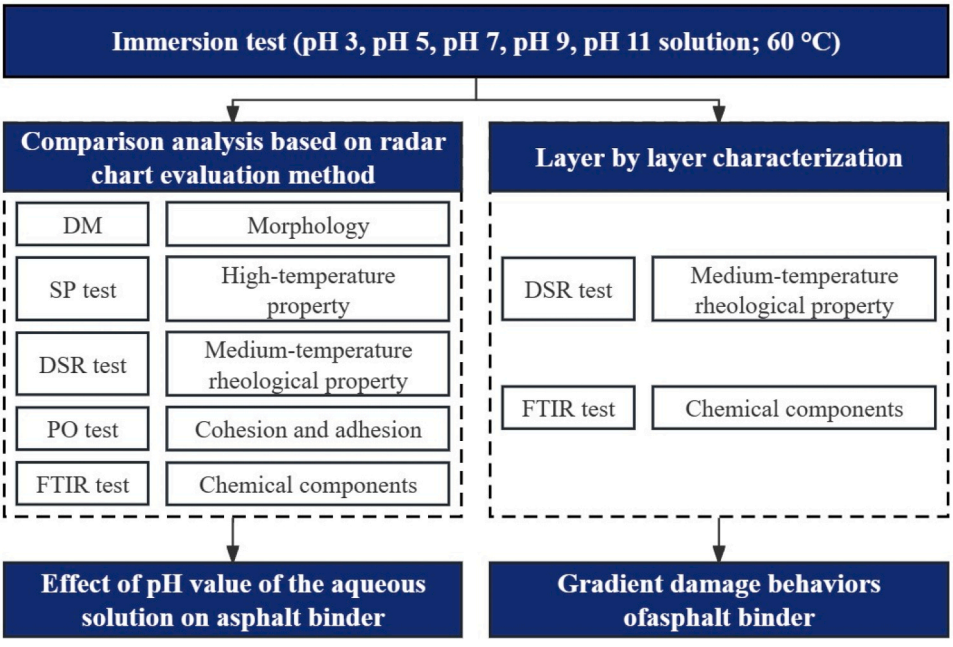

Fig. 1. Research scheme.

the aggregates selected were limestone, basalt, and granite sourced from Wuhan Jiuhua Co., Ltd (Wuhan, China). The basic physical properties of asphalt binders and the chemical components of aggregates were shown in Table 1 and Table 2, respectively.

2.2. Sample preparation

The immersion experiment was used to simulate asphalt binders exposed to wet environments with different pH values. Five kinds of pH solutions were considered in this study, including pH 3, 5, 7, 9, and 11. The pH 3 and 5 solutions were prepared by diluting concentrated sulfuric acid and nitric acid in a molar ratio of 9:1 with distilled water. Distilled water was used for the pH 7 solution. The pH 9 and 11 solutions were prepared by dissolving solid sodium hydroxide in distilled water. Five grams of molten asphalt binder were poured into glass dishes with a diameter of 90 mm and placed in a vacuum oven at 120 °C for 0.5 h to cool and form asphalt films of approximately 0.77 mm thickness. Then, 40 ml of the solutions with different pH values were poured into the glass dishes, allowing the asphalt samples to be fully immersed in the aqueous solutions. Since summer pavement temperatures often reach 60 °C, the test temperature was set to 60 °C to simulate the performance deterioration of asphalt binders exposed to chemical environments with different pH values under high summer temperatures. During immersion, a portable pH meter was used to measure the pH value of the aqueous solutions daily. If pH changes were detected, the immersion solutions were replaced with freshly prepared solutions. After immersion, the asphalt film surfaces were gently rinsed with distilled water to remove residual chemical solutes. Then the films were placed in a 110 °C convection oven for 30 min to remove water from the asphalt film surfaces. To distinguish the effects of solution exposure and temperature during immersion, control samples were obtained by heating under the same conditions without immersion. Because of the small effect depth of the aqueous solution, the surface asphalt was extracted by organic solvent stripping method and prepared as a sample to be tested in order to avoid the influence of the unaffected asphalt in the test on the results. First, 5 ml of trichloroethylene was added to dissolve the surface of the asphalt films. The asphalt solutions were placed in a fume hood for 72 h, followed by vacuum oven drying at 50 °C for 12 h to completely evaporate the trichloroethylene. The FTIR test of dissolved asphalt binder was used to ensure that trichloroethylene was completely volatilized. The dissolution time was adjusted according to the required sample thickness, and the film thickness was calculated using Eq. (1) based on the extracted asphalt mass.

$$T = \frac{m}{\pi r^2 \rho} \tag{1}$$

Where T and m are the thickness and mass of asphalt film, respectively; ρ is the density of asphalt binder; r is the radius of the glass dish.

The asphalt film thickness in asphalt pavement is determined by the asphalt content and aggregate surface area. The theoretical value calculated by the normative formula is approximately 6–15 μm [29]. However, the distribution of asphalt binder is non-uniform in actual application. The 0.1–2 m thick of asphalt film was used for hydrostatic exposure tests in several studies, no rationale or specification was given for their selection [29–31]. Therefore, the asphalt film with a thickness of 0–100 μm on the surface was selected as the research object. Finally, the samples at 0–25 μm, 25–50 μm, and 50–100 μm were prepared for testing.

Table 1
Physical properties of asphalt binders.

Technical information	Units	90 A	SBS MA	Methods
Penetration (25 °C)	0.1 mm	91.5	64.8	ASTM D5[25]
Softening point	°C	44.3	72.1	ASTM D36[26]
Ductility (10 °C /5 °C)	cm	90.2	61	ASTM D113[27]
Solubility (trichloroethylene)	%	99.7	99.6	ASTM D2042[28]

Table 2
Chemical components of limestone, basalt, and granite.

Aggregate	Content (%)						
	SiO_2	CaO	Al_2O_3	Fe_2O_3	MgO	Other	Loss
Limestone	6.31	42.18	2.15	0.64	6.13	0.63	41.96
Basalt	43.56	8.13	15.10	11.67	9.64	8.39	3.51
Granite	72.04	1.82	14.42	1.22	0.71	5.16	4.63

2.3. Characterization methods

2.3.1. DM

Visual measurement technology has been widely applied in various fields due to its unique advantages of non-contact and high precision [32]. A monocular metallurgical microscope (DM3, XINNDA, China) was employed to observe the surface morphology of asphalt binders after immersion in aqueous solutions of different pH values. The working current (WC) was set at 366 mA, the magnification (mag) was 20X, and the working distance (WD) was 20 mm.

2.3.2. SP test

The high-temperature physical property of asphalt binder was characterized by the SP. The asphalt at 0–25 μm obtained from stripping method was heated to the molten state and then poured into the specimen ring to prepare the sample. After 30 min at room temperature, a hot scraper was used to remove excess sample surface, so that the sample surface was flush with the sample ring. The specimen ring was placed at 5 °C for 15 min, and then the test was conducted according to the ASTM D36 criterion [26]. The parallel test set for the test consisted of four samples.

2.3.3. DSR test

The medium-temperature rheological properties and crack resistance of the asphalt binder after immersion in different aqueous solutions were evaluated using a DSR (Smartpave 102, Anton Paar Co., Germany). The samples at 0–25 μm, 25–50 μm, and 50–100 μm were selected for the DSR test. The temperature scans from –10 to 30 °C were performed on the immersed asphalt samples. The deformation was measured under fixed frequency sinusoidal loading of 10 rad/s and characterized by the complex shear modulus (G*) and phase angle (δ) [33]. The asphalt binder was prepared into samples with a diameter of 8 mm and a thickness of 2 mm. The measurements were conducted with a heating rate of 2 °C/min, and strain control of 0.5% [34]. According to the PG grading test method, the G* and δ of 90 A and SBS MA were considered at 28 °C and 25 °C, respectively. The calculation method of temperature was shown in the Eq. (2) [35].

$$T_c = \frac{T_h - T_l}{2} + 4 \tag{2}$$

Where T_c is the temperature being considered; T_h and T_l are the high temperature grade and low temperature grade of asphalt, respectively.

2.3.4. PO test

The PO test was used to characterize the evolution of adhesion and cohesion at the asphalt binder-aggregate interface under different pH aqueous solution environments [36,37]. The samples at 0–25 μm were selected for the PO test. The test mainly consisted of the following 7 steps, as shown in Fig. 2:

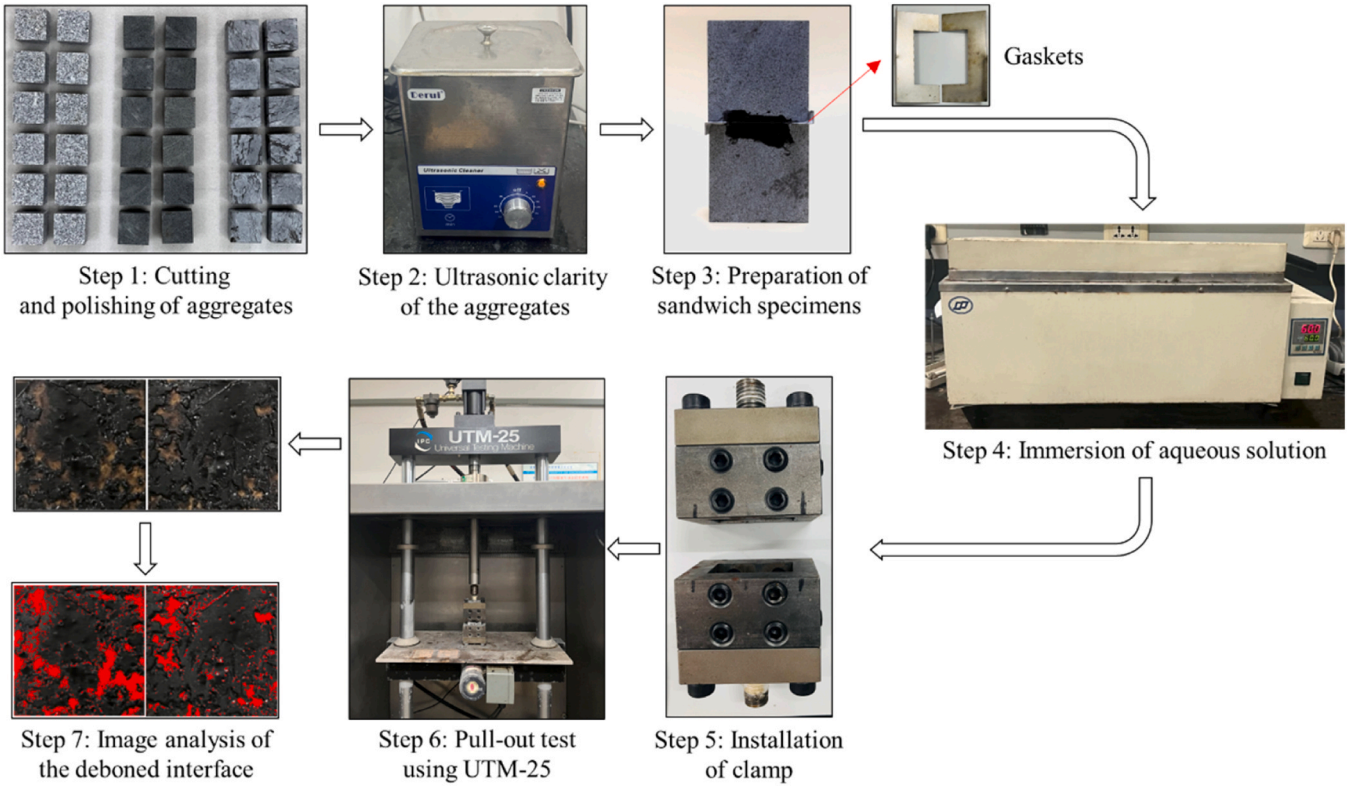

Fig. 2. Procedures for the PO test.

1. Limestone, basalt, and granite were cut into blocks with dimensions of 30 mm × 50 mm× 50 mm, and polished to eliminate the influence of surface roughness.
2. The aggregate blocks were placed in an ultrasonic cleaner for 30 min to avoid residual particles and microorganisms on the aggregate surfaces.
3. The cleaned aggregate blocks were placed in a convection oven at 160 °C for 4 h to ensure complete water evaporation, and the aggregate blocks were also heated to the asphalt mixing temperature. The 30 mm × 50 mm surface of the aggregate blocks was chosen as the test surface. Then the gaskets with a thickness of 0.2 mm and a width of 10 mm were placed at the edges of the test surface to ensure the consistent thickness of asphalt binder for each sample. An appropriate amount of molten asphalt binder was placed on the test surface, the size of which was 30 mm ×30 mm. Pressure was applied by another aggregate block of the same type on the test surface to extrude a sandwich-structured specimen with aggregate-asphalt binder-aggregate. After the sandwich specimens were cured at room temperature for 4 h, the gaskets were removed.
4. The sandwich specimens were immersed in different aqueous solutions (with pH 3, pH 5, pH 7, pH 9, and pH 11) and kept at 60 °C in a water bath for 24 h. Then the specimens were kept at 40 °C in a convection oven for 24 h to ensure dry surfaces. Next, the specimens were conditioned at − 10 °C in the UTM environmental chamber for 4 h.
5. To avoid damage during installation, the clamps were first mounted in the UTM instrument. The sandwich specimens were then embedded in the clamps and fixed with screws.
6. The test parameters were set in the UTM software. A tensile force at 50 mm/min was applied on the top clamp, and the data was collected at 0.01 s intervals to record the force-displacement curve. The test was stopped when interface failure and debonding occurred. Parallel tests were performed 3 times for each sample.
7. The two debonding aggregate surfaces were photographed and the debonding area was calculated by image processing using Image Pro Plus software.

After the PO test, the force-displacement curve of the sandwich specimens was shown in Fig. 3. The force and displacement corresponding to point A, which is the displacement at interface failure, are defined as σ_{max} and ε_{max} [38]. Fracture energy (FE) is a measure of the ability to resist crack propagation and is the energy required for the material to fracture. The higher the FE, the greater the resistance to cracking. FE was calculated by integrating the area under the force-displacement curve, as shown in Eq. (3).

$$FE = \frac{\int_0^{D_{max}} FdD}{S} \tag{3}$$

where F is the axial force corresponding to the displacement; ε is the

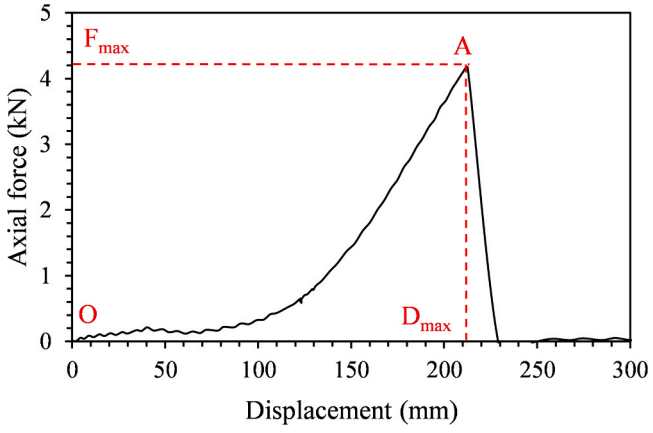

Fig. 3. Force-displacement of sandwich specimens.

displacement change of sandwich specimens; S is the area of the fracture surface.

The area of aggregate uncovered by asphalt binder ($S_{uncovered}$) and the entire interfacial area (S_{total}) were calculated by Image Pro Plus software. The proportion of the debonding area (S_{ratio}) to the interfacial area was further calculated according to Eq. (4) [39]. When the percentage was more than 50% then it was judged as adhesion failure and vice versa.

$$S_{ratio} = \frac{S_{uncovered}}{S_{total}} \tag{4}$$

2.3.5. FTIR test

FTIR (Nicolet 6700, Thermo Fisher Scientific, Waltham, MA, USA) was used to characterize the chemical composition of asphalt binder after immersion in solutions of different pH values. The FTIR test conducted on asphalt samples at 0–25 μm, 25–50 μm, and 50–100 μm. The 10 wt% asphalt was added to the CS_2 solution, then 3 drops of which were dropped on the KBr chip. A heat lamp was used to apply thermal radiation to ensure complete evaporation of the carbon disulfide from the samples [40]. The samples were scanned 64 times over a range of 4000–400 cm^{-1} [41]. The carbonyl index ($I_{C=O}$), sulfoxide index ($I_{S=O}$), and vinyl index ($I_{C=C}$) were used as indicators to characterize the changes in asphalt chemical components, calculated using Eqs. (5)–(7) [42,43].

$$I_{C=O} = \frac{A_{1700\ cm^{-1}}}{\Sigma A_{2000-600\ cm^{-1}}} \tag{5}$$

$$I_{S=O} = \frac{A_{1030\ cm^{-1}}}{\Sigma A_{2000-600\ cm^{-1}}} \tag{6}$$

$$I_{C=C} = \frac{A_{966\ cm^{-1}}}{\Sigma A_{2000-600\ cm^{-1}}} \tag{7}$$

where $A_{1700cm^{-1}}$, $A_{1030cm^{-1}}$ and $A_{966cm^{-1}}$ are the area of C═O, S═O and C═C at the 1700 cm^{-1}, 1030 cm^{-1} and 966 cm^{-1} respectively; $\Sigma A_{2000-600cm^{-1}}$ is the total area integral area between the infrared spectral curve from 2000 cm^{-1} to 600 cm^{-1} and the baseline.

2.3.6. Radar chart analysis method

The radar chart analysis method is an intuitive multi-indicator analysis and decision-making method [44]. It uses the graphical area of radar charts to judge the pros and cons of different schemes. The improved radar chart analysis method was cited to evaluate various property indicators of asphalt binders under aqueous solution environments of different pH values, comprehensively reflecting the degradation of asphalt binder in the environment. In the first step, vector $X = \{x_1, x_2, \ldots, x_n\}$ and vector $Y = \{y_1, y_2, \ldots, y_n\}$ were used to represent a group of objects to be evaluated and a group of corresponding indicators respectively, thus establishing matrix $A = (a_{ij})_{n\times k}$ ($i = 1,2, \ldots, n$; $j = 1,2, \ldots, n$). In the second step, Eq. (8) and (9) were used to standardize and nonlinearly transform the matrix data respectively [45].

$$b_{ij} = \frac{a_{ij} - E(y_j)}{\sigma(y_j)} \tag{8}$$

$$r_{ij} = \frac{2}{\pi}\arctan\left(b_{ij}\right) + 1 \tag{9}$$

where a_{ij} and b_{ij} are the indicators in the matrix and the standardized matrix, respectively; $E(y_j)$ and $\sigma(y_j)$ are the mean and standard deviation of indicator j; r_{ij} represents the j evaluation index of the evaluation object after the non-linear transformation.

after the basic indicator non-linear transformation.

In the next step, the characteristic vector was calculated using Eqs. (10) and (11).

$$u_i = [A_i, L_i] \tag{10}$$

$$\begin{cases} A_i = \sum_{j=1}^{k} \frac{1}{k}\pi r_{ij}^2 \\ L_i = \sum_{j=1}^{k} \frac{2}{k}\pi r_{ij} \end{cases} \tag{11}$$

where u_i and k are the evaluation vector of evaluation object i, and the number of indicators; A_i is the area of the radar chart, representing the integrated level of objective i; L_i is the perimeter of the radar chart, representing the difference between the indicators; and k is the number of indicators.

Finally, the evaluation vector was determined based on the aforementioned characteristic vector, thereby deriving the comprehensive evaluation function. The calculation formula was shown in Eqs. (12)–(14).

$$e_i = [e_{i1}, e_{i2}] \tag{12}$$

$$\begin{cases} e_{i1} = \frac{A_i}{MaxA_i} \\ e_{i2} = \frac{L_i}{2\pi\sqrt{\frac{A_i}{\pi}}} \end{cases} \tag{13}$$

$$f(e_{i1}, e_{i2}) = \sqrt{e_{i1} \times e_{i2}} \tag{14}$$

where e_{i1} and e_{i2} are the relative area and perimeter, and f is the comprehensive assessment index.

3. Results and discussions

3.1. Effect of pH value of the aqueous solution on the morphology of asphalt binder

Based on previous studies, the effect of 21 d exposure on asphalt binder is more obvious [46]. Therefore, the morphology of the asphalt binder exposed to different chemistry for 21 d of immersion in aqueous solutions with different pH values was investigated by DM, as illustrated in Fig. 4. The surface of 90 A exposed to pH 3 formed a film full of wrinkles, and the film was torn to show a clear wide crack, with the black area representing the exposed internal asphalt binder. The pH 5 solution caused small cracks to appear on the rough surface of 90 A. The pH 7 solution caused the surface of 90 A to become looser, revealing more internal asphalt binder. The small cracks appeared on the smooth surface of 90 A exposed to pH 9, and the white particles on the surface might be NaOH crystals or the salt produced by a saponification reaction between asphalt and NaOH solution [47]. The pH 11 aqueous solution caused the surface of 90 A to develop a denser mesh of cracks. It indicated that the surface of 90 A was most severely eroded by the pH 3 solution, causing a plastic film to form on the surface, which further invaded the interior by tearing the surface film. The surface components were partially dissolved by the pH 5 and pH 7 aqueous solutions gradually. The fine cracks on the 90 A exposed to pH 9 and pH 11 may be the result of the sodium hydroxide solute in the aqueous solution penetrating the surface, as crystals still appeared after the surface was cleaned.

The surface of SBS MA control evenly distributed white dots, which might be the uniform distribution of SBS. The surface of SBS MA exposed to pH 3 was rough and accompanied by small cracks, while the surface of SBS MA exposed to pH 5 revealed plush cracks with greater roughness in the center of the cracks. The surface morphology of SBS MA exposed to pH 7, 9, and 11 was similar with a slight increase in surface roughness. It suggests that SBS MA is most seriously eroded by the pH 3 solution,

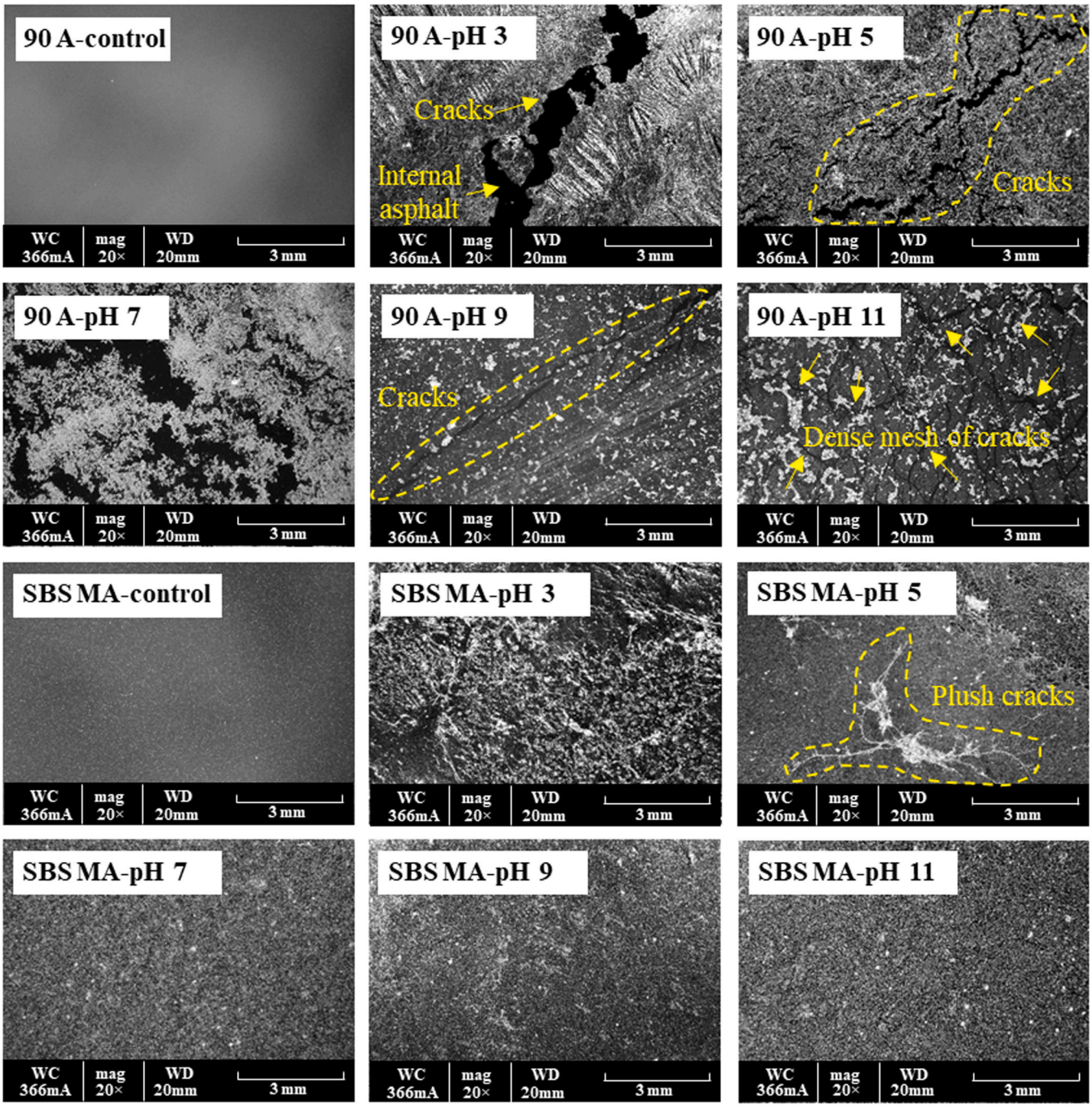

Fig. 4. Morphology of asphalt binders exposed to aqueous solution with different pH values for 21 days.

which might be acidic solutes tearing the SBS MA surface and further invading to make the surface rough. The surface morphology of SBS MA was not significantly affected by the pH 7, 9, and 11 aqueous solutions. After exposure to aqueous solution, the surface morphology of SBS MA was significantly smaller than that of 90 A. It was possible that the uniform distribution of SBS on the surface of SBS MA prevented the loss of asphalt components.

3.2. Effect of pH value of the aqueous solution on physicochemical properties of asphalt binder

3.2.1. High-temperature property of asphalt binder

The softening points of asphalt binders were compared to analyze the effect of pH value on the high-temperature property, as illustrated in Fig. 5. The points and bars were the test data and error bars of data, respectively. The experimental results are average values with standard errors. The softening points of asphalt binder exposed to aqueous solutions for 21 days exhibited varying degrees of reduction, implying the solutions softened the asphalt binder. The similar softening points of 90 A after exposed to pH 3, 5, and 7 solutions indicated that the high-temperature property was predominantly affected by moisture rather than the pH value of the acid solution. However, the softening point increased with the ascending pH value of the alkaline solutions, suggesting that the presence of alkaline solutes inhibited moisture exposure of 90 A. The softening point of SBS MA decreased with a reducing pH value, demonstrating greater sensitivity to acidic solutions. This could be attributed to the chemically degraded into small molecules by the acid solution and the destruction of the SBS network structure [48]. The

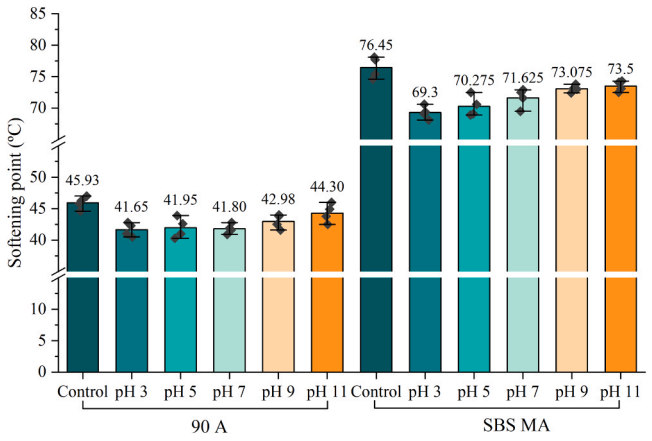

Fig. 5. Softening point of the asphalt binder before and after immersion for 21 days.

pH 3 solution reduced the softening point of 90 A and SBSMA by 9.32% and 9.35%, respectively. SBS MA was more sensitive to the pH value of aqueous solution compared with different pH values. This showed that SBS reacted more easily with aqueous solution than asphalt molecules.

3.2.2. *Medium-temperature rheological property of asphalt binder*

The medium-temperature rheological properties of asphalt binder were characterized by the G* and δ, as shown in Fig. 6. The G* is the ratio of the maximum shear stress to the maximum shear strain, the index of the total resistance of a material to repeated shear deformation [49]. A larger G* indicates that the asphalt has a stronger resistance to deformation. The δ is related to the time lag between the stress and the strain, reflecting the viscoelastic ratio of asphalt [34]. The greater the δ, the greater the viscosity, the better the asphalt flow properties. From Fig. 6a, the G* of asphalt binder decreases with rising temperature, while the δ elevates with increasing temperature. This is determined by the viscoelastic properties of asphalt binder under different temperature conditions, indicating that the rheological behavior of asphalt binder changes from elastic to viscous. After the exposure of the aqueous solution, the G* decreases, and the δ increases. The pH 7 solution has the greatest effect, and the G* gradually increases to the proximity of that of the control sample as the pH value decreases or increases. The change rule of δ with pH was opposite to that of G*. It indicated that water gradually transformed the asphalt from elastic to viscous state. This might be because the dissolving and migrating effects of water on asphalt dominate at this stage. Previous studies have shown that asphalt oxidation generally occurs in the pre-exposure period, while asphalt dissolution and migration will dominate in the later period [17,18,24]. In contrast to the pH 7 solution, the addition of acid and alkali solutes hindered the asphalt binder from changing from elastic to viscous, and delayed the attenuation of asphalt deformation resistance.

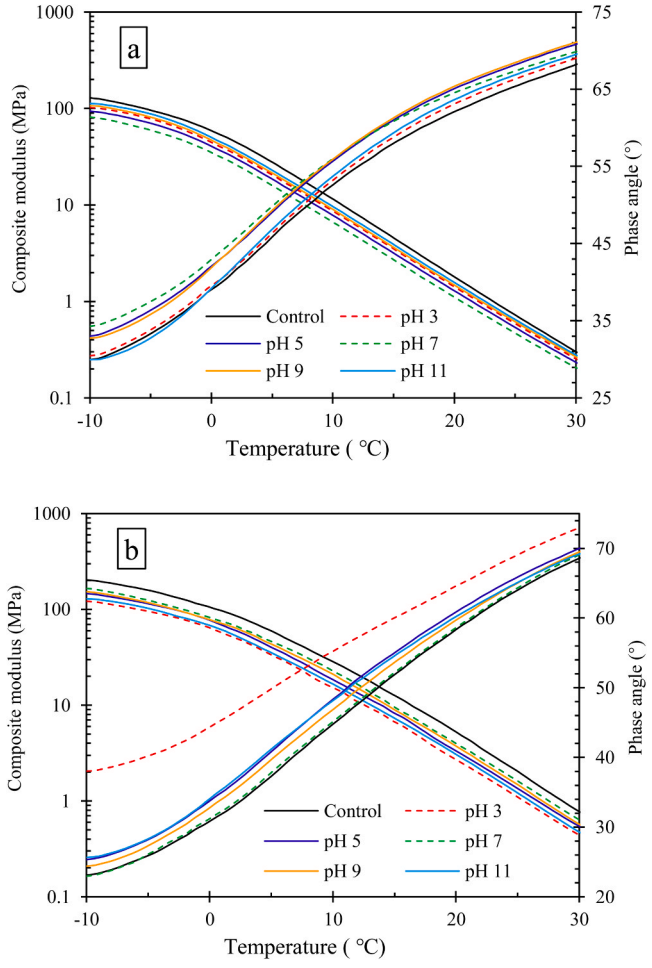

Fig. 6. G* and δ of the asphalt binder before and after immersion for 21 days (a, 90 A; b, SBS MA).

From Fig. 6b, the G* of SBS MA reduced while the δ of SBS MA increased after immersion in different solutions. The G* of SBS MA exposed to the pH 3 solution is the lowest, while the G* increases gradually when the pH value increases to 7. With a further increase in pH value, the G* of SBS MA decreases sequentially. The deformation resistance of SBS MA was further weakened by acid and alkali solutes, which was the result of the chemical reaction between SBS and solutions leading to a reduction in SBS content. The δ of SBS MA exposed to different solutions increased in the opposite trend to the G*. These results indicated that both acid and alkali solutes could promote the transformation of asphalt from elastic to viscous.

In order to quantify the effect of different pH values on the G* and δ, the change degree in the G* and δ of 90 A and SBS MA at 28 °C and 25 °C was quantified, as shown in Table 3. It could be found that the degradation degree of 90 A resistance to deformation by pH 7 solution was 1.95 times more than that by pH 3 solution and 3.84 times more than that by pH 11 solution. And the order of magnitude of the effect of different pH value on the δ was as follows, pH 9 > pH 5 > pH 7 > pH 11 > pH 3. This indicated that the asphalt viscoelastic component was more affected by the alkali solute, but the effect decreased with increasing solute concentration. The weakening effect of acid and alkaline solutions on the deformation resistance of SBS MA was very significant, with that of pH 3 solution and pH 11 solution acting 2.27 and 1.98 times more than that of pH 7 solution, respectively. In addition, pH 3 solution and pH 11 solution affect the δ of SBS MA to a degree of 15.56 and 3.32 times that of pH 7 solution. Consistent with the softening point test results, the sensitivity of the rheological properties of SBS MA to the pH value of aqueous solution was greater than 90 A.

3.2.3. *Cohesion of asphalt binder and adhesion between asphalt binder and aggregate*

Sandwich specimens exposed to aqueous solutions with different pH

Table 3
Variation of G* and δ of asphalt exposure to aqueous solution (%).

pH value	90 A (28 °C)		SBS MA (25 °C)	
	G*	δ	G*	δ
pH 3	-16.96	1.31	-46.37	7.78
pH 5	-23.52	4.03	-34.03	2.87
pH 7	-33.07	2.67	-20.44	0.50
pH 9	-12.92	4.42	-27.33	1.59
pH 11	-8.61	2.06	-40.55	1.66

values were tested in PO tests to obtain the interfacial FE, and the S_{ratio} in chemical environments was quantitatively characterized, as depicted in Fig. 7. The FE of the 90 A-aggregate interfaces were all significantly reduced after aqueous solution exposure, with pH 7 causing the least damage to the interfacial FE. For 90 A-limestone, the FE was more sensitive to pH 11 and pH 3, which reduced the FE by 81.47% and 68.23%, respectively. The interfacial failures were adhesion failures, with the S_{ratio} changes within 5% across solutions, indicating minimal pH effect on the 90 A-limestone interfacial failure type. For 90 A-basalt, the interfacial FE at dry was larger than that of 90 A-limestone, attributed to basalt's surface with tiny pores. Cohesion failure occurred in pH 5 and pH 7 environments and the S_{ratio} reached a minimum of 27.54% in pH 7 environments, but the FE was similar to that of the control. It suggested that the main damage to the interface was adhesion rather than cohesion. This is because the surface was rich in pores, and the embedded structure was formed after asphalt infiltration. The interface FE and S_{ratio} in pH 3 and pH 5 environments were smaller than those in pH 9 and pH 11 environments. It indicated that the acid solution had a greater degree of damage to cohesion. Both pH 9 and pH 11 solutions made the S_{ratio} larger than the control, indicating that the alkali solution was more likely to cause interface adhesion damage. The 90 A-granite interfaces showed the smallest FE due to granite's smooth and non-porous surface with $>$ 66% SiO_2 content, making it acidic with poor physical and chemical interaction with the acidic asphalt binder. The interfacial cohesion was easily damaged by acid solutions, while the interfacial adhesion was easily damaged by alkali solutions..

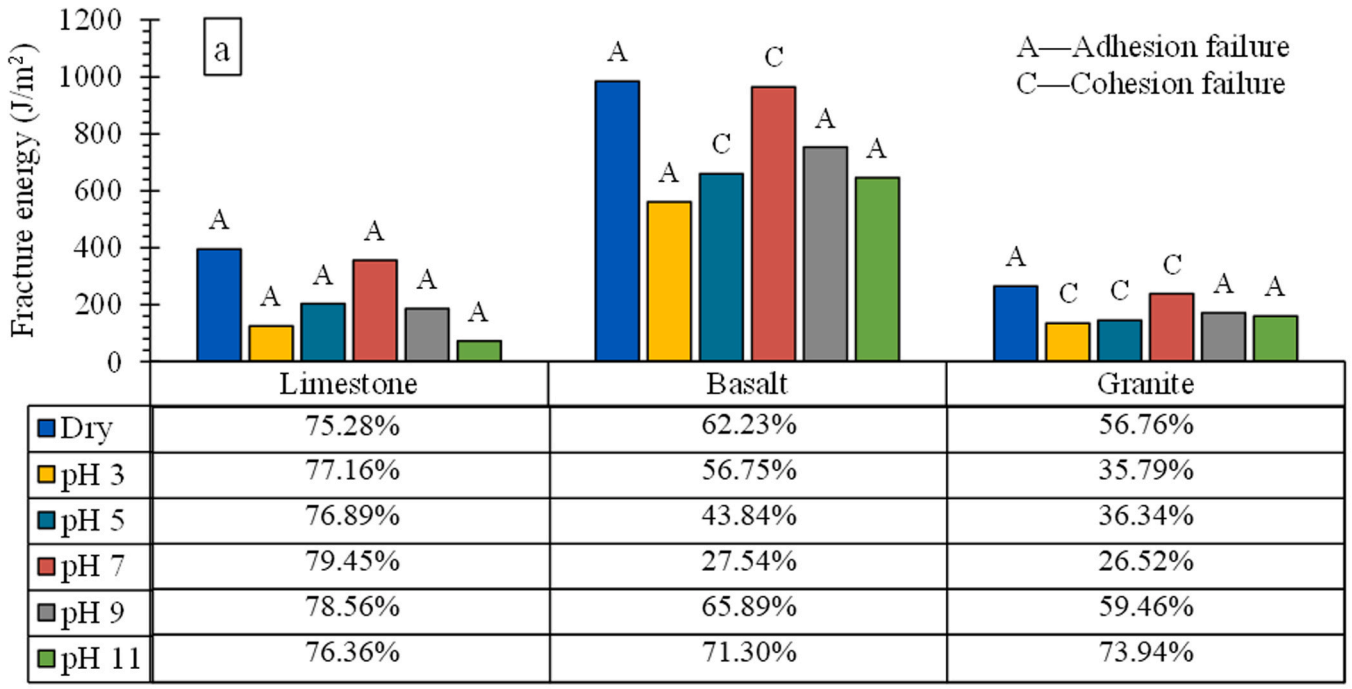

	Limestone	Basalt	Granite
Dry	75.28%	62.23%	56.76%
pH 3	77.16%	56.75%	35.79%
pH 5	76.89%	43.84%	36.34%
pH 7	79.45%	27.54%	26.52%
pH 9	78.56%	65.89%	59.46%
pH 11	76.36%	71.30%	73.94%

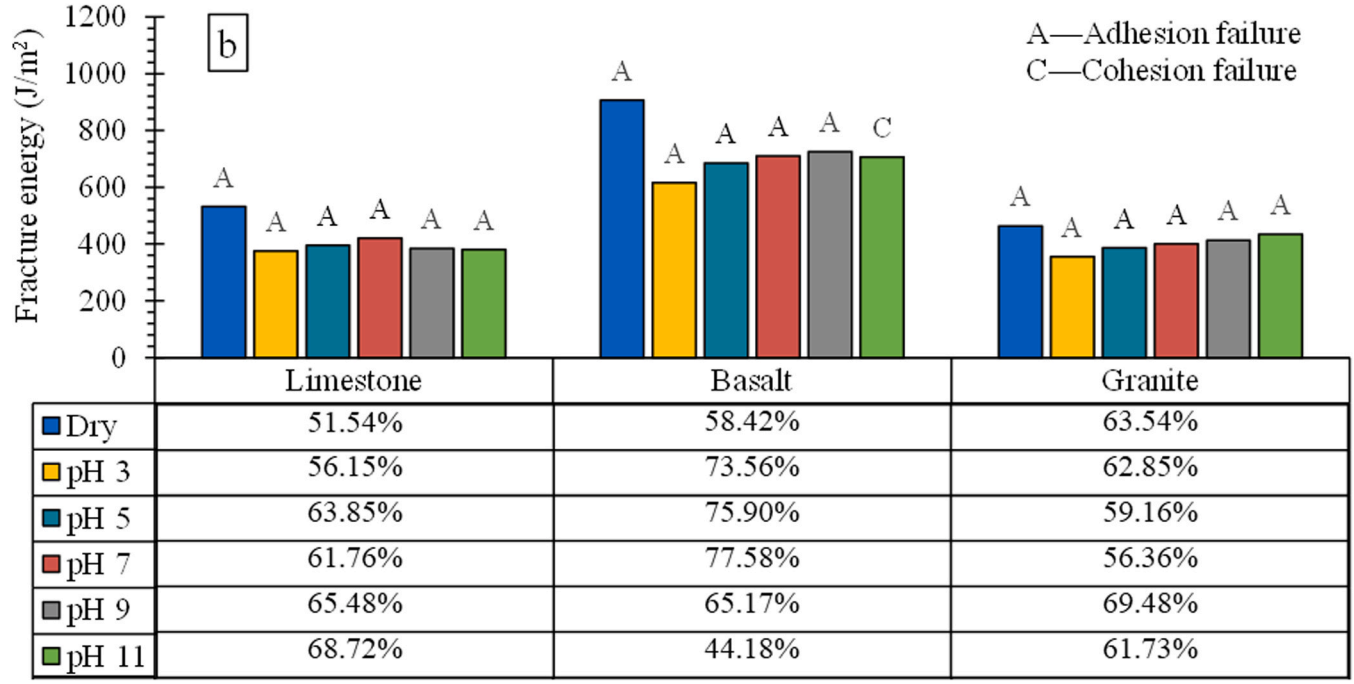

	Limestone	Basalt	Granite
Dry	51.54%	58.42%	63.54%
pH 3	56.15%	73.56%	62.85%
pH 5	63.85%	75.90%	59.16%
pH 7	61.76%	77.58%	56.36%
pH 9	65.48%	65.17%	69.48%
pH 11	68.72%	44.18%	61.73%

Fig. 7. FE between asphalt binder and aggregate in aqueous solution with different pH values for 21 days (a, 90 A; b, SBS MA).

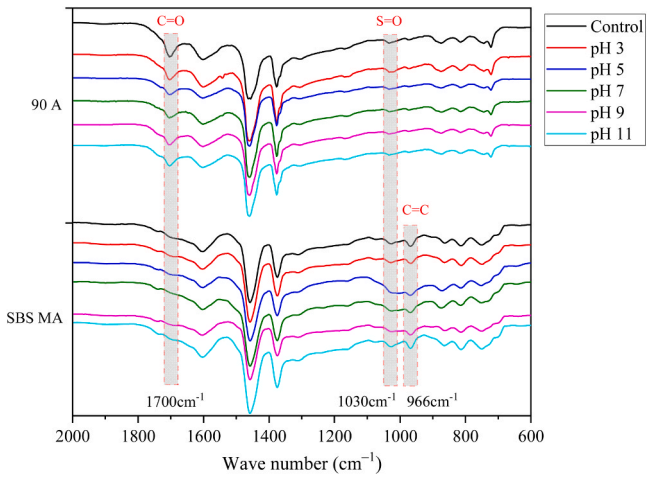

Fig. 8. FTIR spectrum of asphalt binder after immersion for 21 days.

The interfacial adhesion failure occurred between SBS MA and limestone under wet conditions, with the fracture energy (FE) unaffected by pH value (changes within 5%). The S_{ratio} increased slightly with increasing pH value, indicating that the pH value manifested a slight negative effect on interfacial adhesion. Except for the SBS MA-basalt in the pH 11 environment, the FE of the SBS MA-basalt interface and SBS MA-granite interfaces increased with the ascending pH value, and both of them were adhesion failures. Their FE was reduced by 32.00% and 23.11% in pH 3 environments, respectively. The S_{ratio} of SBS MA-basalt decreased as the pH value increased, approaching 50% at pH 11. This indicated that the cohesion damage and adhesion damage to the SBS MA-basalt interface increased, and the adhesion damage to the SBS MA-granite interface decreased with rising pH values. Potentially, alkali solutions promote the emulsification between the asphalt binder and water, weakening the cohesion bonds within the asphalt binder [50]. The FE of SBS MA-aggregate after exposure to aqueous solution was basically greater than that of 90 A-aggregate, indicating that the network structure of SBS polymer enhanced the adhesion between asphalt and aggregate. The S_{ratio} of SBS MA-limestone was less than 90A-limestone, manifesting the cohesion of SBS MA-limestone was greater than 90 A. In addition, the SBS MA-aggregate interface had the stronger resistance to effect of aqueous solutions, and was less affected by pH value.

3.2.4. Chemical component of asphalt binder

After exposure to the aqueous solution with different pH values, the FTIR spectrums of asphalt samples were characterized, as displayed in 0. Obvious changes occurred in some peaks at 1700 cm^{-1} and 1030 cm^{-1}, representing carbonyl and sulfoxide groups. They are often used as the main oxidation products of asphalt binders to observe oxidation, dissolution, and migration. The characteristic peak at 966 cm^{-1} in SBS MA is also a key peak, formed by the out-of-plane rocking vibrations of the C–H segments of the olefin (C═C) in trans-butadiene. It can be used to characterize the degree of degradation of SBS. To avoid subjective visual judgment limitations, the characteristic peak indexes were calculated, as shown in Fig. 9. The points and bars were the test data and error bars of data, respectively. The experimental results are average values with standard errors. After exposure to the aqueous solutions, the $I_{C=O}$ of 90 A decreased, and the $I_{S=O}$ increased. This might be because the polar component is stripped by dissolution reducing the $I_{C=O}$. Meanwhile, the olefins in the asphalt binder underwent esterification with sulfuric acid to form sulfites or sulfates. Then the cationic intermediates formed by their reaction with the isomeric alkanes reacted with the olefins to produce long-chain isomeric alkanes with sulfoxide groups [19]. The $I_{C=O}$ first decreased then increased with pH value, reaching the maximum and minimum at pH 7 and pH 11, respectively. The $I_{S=O}$ decreased with increasing pH value, that of the sample exposed to pH 3 solution increased by 52.67%, while that of the sample exposed to pH 11 increased by 9.56%. This indicated that the chemical component of 90 A was more sensitive to the aqueous solutions with low pH values.

The $I_{C=O}$ of SBS MA exposed to aqueous solution increased, with increases of 41.04% and 63.54% at pH 9 and 11, respectively. The $I_{S=O}$ fluctuated up and down with pH value, decreasing by 8.57% at pH 3 and increasing by 35.91% at pH 7. The $I_{C=C}$ decreased at wet but increased then decreased with pH value, with decreases of 17.88% and 17.09% for pH 3 and 11 solutions, respectively. It indicated that acid solution and alkaline solution promoted the oxidation of asphalt binder and the degradation of olefinic double bonds in butadiene. It could be seen that the C═O and S═O change to a lesser extent than C═C, indicating that SBS molecules were more susceptible to attack by pH 3 acidic solutions than 90 A asphalt molecules. The underlying mechanism is that the ester bonds in SBS can be hydrolyzed by the acid solution to form carboxylic acids and alcohols [48]. Additionally, SBS can undergo sulfidation reactions with sulfuric acid to generate sulfoxides, which destroys the micro-phase separation structure of SBS, weakening its compatibility with asphalt. This might be the reason why the phase angle of SBS MA affected by acid solution is greater than 90 in Fig. 6.

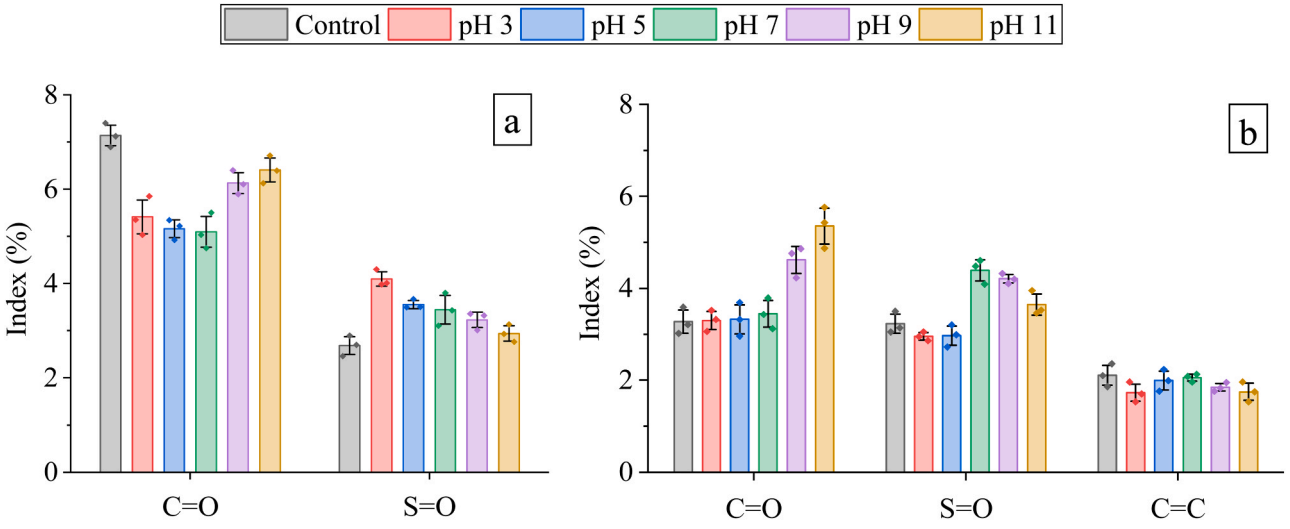

Fig. 9. Characteristic peak indexes of asphalt binder after immersion for 21 days (a, 90 A; b, SBS MA).

3.3. Comparison analysis based on radar chart evaluation method

The radar chart analysis method was conducted to comprehensively evaluate the effect of the pH value of the aqueous solution on the physicochemical properties of 90 A and SBS MA. Nine evaluation indexes including softening point (SP), G* , δ, FE with limestone (FE_l), fracture energy with basalt (FE_b), fracture energy with granite (FE_g), $I_{C=O}$, $I_{S=O}$, and $I_{C=C}$ were incorporated into the radar charts. The nine indicators in the 12-group matrix A were given in Table 4.

The indicators are subsequently normalized and non-linearly transformed then plotted as radar charts as in Fig. 10. The charts visualized the effect of pH value on the physicochemical properties of asphalt binder, with larger sector areas indicating greater index values. The variations of δ, FE_l, FE_b, FE_g, $I_{C=O}$, $I_{S=O}$, and $I_{C=C}$ are more obvious in the environment chemistry. The dissolution and migration of asphalt binder exposed to the aqueous solution leads to a decrease in the polar components and an increase in the viscous components. Hence, the adhesion between asphalt binder and aggregate is markedly weakened. The charts demonstrated that the effect of the aqueous solution on the property indexes of 90 A and SBS MA was more significant at extreme acidic/alkaline pH levels. Furthermore, SBS MA exhibited substantially higher chemical resistance than 90 A. Optimal asphalt types can thus be selected from the radar charts when designing asphalt pavements targeting enhanced performance.

The evaluation vector was calculated, as tabulated in Table 5. The comprehensive evaluation function (*f*) results across the 12 sample groups are plotted in Fig. 11. The results showed that the *f* of all samples decreased after the exposure to the aqueous solution. The pH 3, pH 5, pH 7, pH 9, and pH 11 solutions reduced the *f* of 90 A by 20.8%, 20.2%, 1.5%, 14.0%, and 25.5%, respectively. It signified that the properties of 90 A were affected by the acid solution significantly, though the pH of the acids had minimal impact. In contrast, 90 A exhibited greater sensitivity to alkali solutions, and the greater the pH value of the alkali solution, the greater the degree of damage. For SBS MA, the pH 3, pH 5, pH 7, pH 9, and pH 11 solution decreased the *f* by 23.2%, 17.7%, 4.6%, 8.7%, and 13.0%, respectively. It demonstrated that the existence of acid and alkali solute aggravated the damage of aqueous solution to asphalt properties, and the effect of acid solute was greater than that of alkaline solute.

3.4. Gradient damage behaviors of asphalt binder exposed to the aqueous solution with different pH value

To investigate the gradient damage behaviors of properties of asphalt binder, asphalt surface layers of 0–25 μm, 25–50 μm, and 50–100 μm were stripped from asphalt binder after immersion in different solutions for the FTIR test. It can be seen from the above experimental results that the effects of pH 5 and pH 9 were less pronounced than pH 3 and pH 11, but their trends aligned. Thus, irrespective of solute concentration on asphalt properties, pH 3, pH 7, and pH 11 were regarded as acid, neutral, and alkali solutions. Fig. 12 depicted the effect of three factors, including pH value, immersion time (7 days, 14 days, and 21 days), and depth, on the $I_{C=O}$ and $I_{S=O}$ of 90 A. The $I_{C=O}$ of 90 A was most affected by the pH 3 solution to decrease significantly. However, the $I_{C=O}$ at 0–25 μm was greater than at 25–50 μm. It indicated the dissolution and migration of carbonyls occurred within 0–100 μm, while the oxidation reactions to form carbonyls took place at 0–25 μm. As time increased, the oxidation at 0–25 μm was gradually promoted and the carbonyls diffused inward. It weakened the effect of the pH 3 solution on the chemical components of 90 A, suggesting the oxidation reactions to form carbonyls was the major trend under pH 3 aqueous exposure for the long term. After 90 A was exposed to pH 3 for 7 days, the $I_{S=O}$ greatly increased, likely because sulfuric acid reacted with 90 A within 0–50 μm to extensively generate sulfenyl groups. Additionally, the $I_{S=O}$ at 0–25 μm was lower than 25–50 μm, signifying the oxidation to form sulfoxide occurred at 90 A within 0–100 μm, alongside the dissolution and migration of sulfoxide occurred at 90 A within 0–25 μm. The $I_{S=O}$ gradually decreased over time, reaching the value of the control sample at 21 days. It could be seen that carbonyl and sulfinyl groups exhibited some competitive interplay, with opposing tendencies.

The pH 7 solution caused a gradual dissolution and migration of the carbonyl groups in the asphalt binder from the surface to the deeper layers, and the $I_{C=O}$ fluctuated and decreased with time. Meanwhile, the $I_{S=O}$ increased and was not much affected by the immersion time. Nonetheless, the effect of dissolution and migration led to an order of magnitude of the $I_{S=O}$ of 50–100 μm > 25–50 μm > 0–25 μm after 7 days. After 14 days, the generation of the sulfenyl group might dominate, leading to the gradual oxidation of the asphalt binder from the surface to the interior. The $I_{S=O}$ was the smallest at 0–25 μm after 21 days, which suggested that the oxidative, migration, and dissolution of the sulfenyl group alternated cyclically [24].

After 90 A was exposed to pH 11 for 7 days, the $I_{C=O}$ slightly increased in the order of 0–25 μm < 25–50 μm < 50–100 μm. This might be because the oxidation of 90 A accumulated carbonyls within 0–100 μm within 7 days, but gradual dissolution and migration at 0–50 μm led to lower $I_{C=O}$ versus 50–100 μm. As time elapsed, the further dissolution and migration of carbonyls at 0–25 μm caused the carbonyls at 50–100 μm to gradually diffuse into 0–25 μm. The $I_{S=O}$ of 90 A exposed to the pH 3 for 3 days increased, and the $I_{S=O}$ at 0–25 μm was the maximum. It indicated the oxidation reaction to form the sulfoxide group occurred within 0–25 μm. After 14 days, 0–25 μm was lower than 25–50 μm, suggesting the oxidation depth reached

Table 4
Matrices for evaluation indicators of asphalt binder.

Asphalt binder	pH value	High-temperature property	Medium-temperature rheological property		Adhesion			Chemical components		
		SP (°C)	G* (MPa)	δ (°)	FE to limestone (MPa)	FE to basalt (MPa)	FE to granite (MPa)	$I_{C=O}$ (%)	$I_{S=O}$ (%)	$I_{C=C}$ (%)
90 A	Control	45.9	0.3933	67.34	0.40	0.99	0.27	7.14	2.68	NA
	3	42.0	0.3265	68.22	0.13	0.56	0.14	5.41	4.10	NA
	5	41.7	0.3008	70.05	0.20	0.66	0.15	5.16	3.55	NA
	7	41.8	0.2632	69.14	0.36	0.96	0.24	5.09	3.44	NA
	9	43.0	0.3424	70.31	0.19	0.75	0.17	6.13	3.23	NA
	11	44.3	0.3594	68.73	0.07	0.65	0.16	6.41	2.94	NA
SBS MA	Control	76.5	1.9368	64.30	0.53	0.91	0.46	3.27	3.23	2.11
	3	69.3	1.0388	69.30	0.38	0.62	0.36	3.30	2.95	1.73
	5	70.3	1.2777	66.15	0.40	0.69	0.39	3.32	2.97	1.99
	7	71.6	1.5410	64.62	0.42	0.71	0.40	3.45	4.39	2.80
	9	73.1	1.4075	65.32	0.38	0.73	0.41	4.62	4.21	1.85
	11	73.5	1.1515	65.37	0.38	0.71	0.43	5.35	3.65	1.75

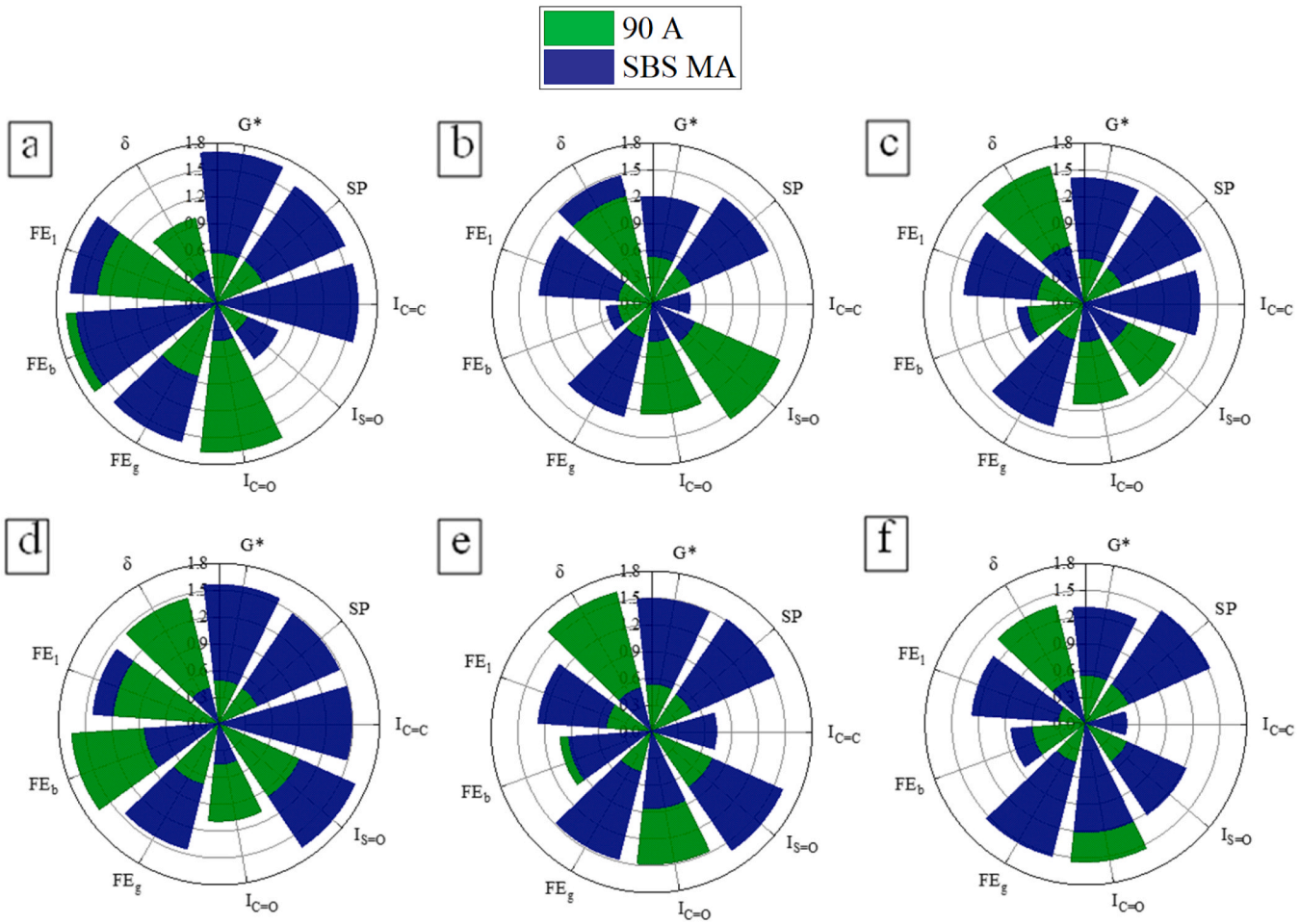

Fig. 10. Radar charts for 90 A and SBS MA responding to pH value (a, control; b, pH 3; c, pH 5; d, pH 7; e, pH 9; f, pH 11).

Table 5
Eigenvectors u_i and evaluation vectors ν_i in the matrix.

Asphalt binder	RAP content (%)	$u_i = [A_i, L_i]$	$\nu_i = [\nu_{i1}, \nu_{i2}]$
90 A	Control	[3.9017, 6.3266]	[0.6782, 0.9035]
	3	[2.5593, 4.8998]	[0.4449, 0.8640]
	5	[2.5052, 5.0297]	[0.4355, 0.8964]
	7	[3.6837, 6.3174]	[0.6403, 0.9285]
	9	[2.9188, 5.4066]	[0.5074, 0.8927]
	11	[2.2679, 4.6040]	[0.3942, 0.8624]
SBS MA	Control	[5.7530, 7.8346]	[1.0000, 0.9214]
	3	[3.4340, 5.9741]	[0.5969, 0.9094]
	5	[3.8556, 6.4833]	[0.6702, 0.9314]
	7	[5.1774, 7.5215]	[0.9000, 0.9325]
	9	[4.6512, 7.2595]	[0.8085, 0.9495]
	11	[4.2467, 6.9050]	[0.7382, 0.9452]

25–50 μm, while the dissolution of the sulfoxide group began at 0–25 μm. After 21 days, the $I_{S=O}$ slightly increased in the order of 0–25 μm < 25–50 μm < 50–100 μm showing the oxidation depth expanded to 50–100 μm.

The characteristic peak indexes of SBS MA samples at different depths were depicted in Fig. 13. The $I_{C=O}$ of SBS MA was minimally unaffected by the pH 3 solution, while the $I_{S=O}$ slightly decreased, with the least $I_{S=O}$ at 25–50 μm. It manifested that the dissolution and migration of SBS MA occurred in 0–50 μm, while the oxidation mainly occurred in 0–25 μm. With prolonged pH 3 exposure, the $I_{C=C}$ declined without obvious depth-dependent patterns. It indicated that SBS was gradually chemically degraded by pH 3 solution, but the degradation state at different depths was related to the distribution of SBS in the asphalt binder.

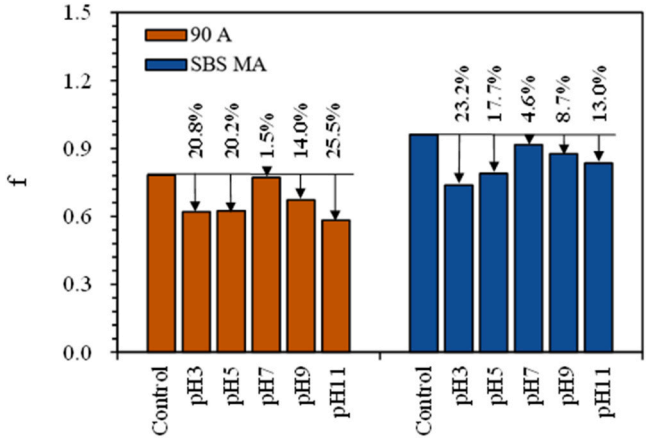

Fig. 11. Comprehensive assessment index of asphalt binder immersed in aqueous solution with different pH values.

After immersion in pH 7 for 7 days, the $I_{C=O}$ of SBS MA increased at 0–50 μm and decreased at 50–100 μm. At 14d and 21d, the $I_{C=O}$ fluctuated around the control values, indicating alternating dissolution, migration, and oxidation of SBS MA. The $I_{S=O}$ first increased then decreased with exposure time in the pH 7 solution and gradually increased with depth, with the $I_{S=O}$ at 50–100 μm greater than 0–50 μm. This suggested the dissolution depth of sulfoxide was 0–50 μm, while the

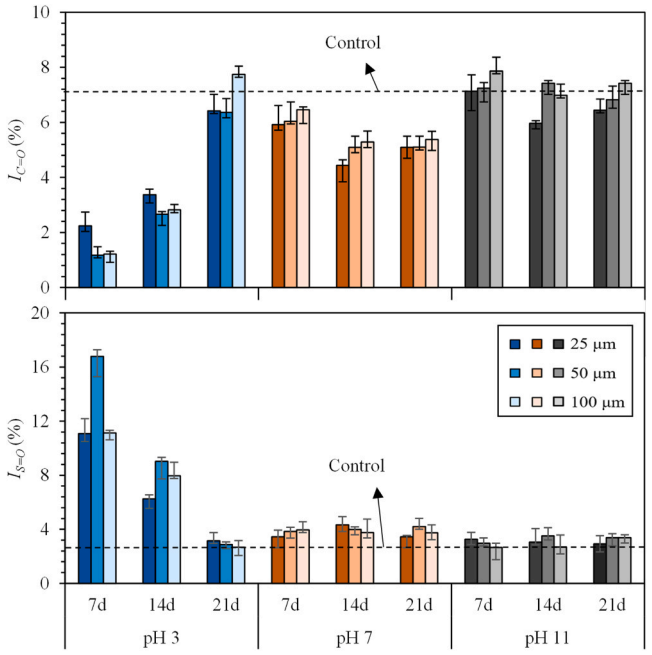

Fig. 12. Characteristic peak indexes of 90 A samples at different depths.

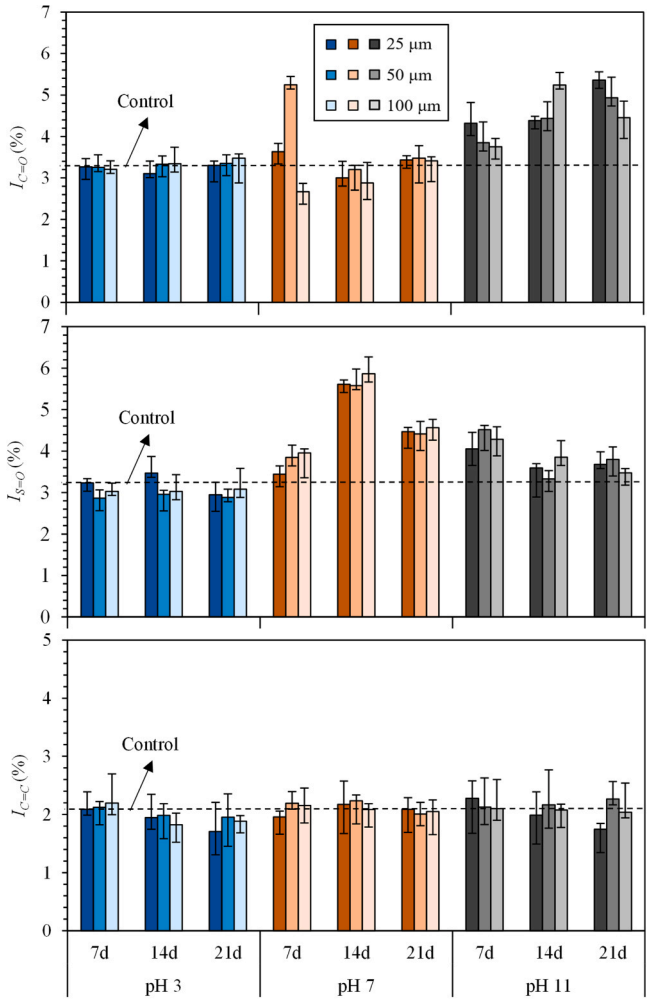

Fig. 13. Characteristic peak indexes of SBS MA samples at different depths.

oxidation depth was 0–100 μm. In addition, the $I_{C=C}$ was barely affected by the pH 7 aqueous solution.

After 7 days and 21 days of exposure to the pH 11 solution, SBS MA at 0–25 μm was oxidized to form the carbonyl, which gradually diffused inward. A certain degree of dissolution of the asphalt binder was generated within 0–50 μm after 14 days. Meanwhile, the carbonyl index elevated gradually with the ascending time. It indicated that the dissolution, migration, and oxidation occurred alternately, but the oxidation reaction that produced the carbonyl group was dominant. As time progressed, the $I_{S=O}$ first increased and then decreased, with 0–50 μm being the most markedly affected. It suggested the effect depth was 0–50 μm, while compositional changes at 50–100 μm depth were caused by diffusion from 0–50 μm. The slight decrease of $I_{C=C}$ at 0–25 μm after 21 days signified that the pH 11 solution had a smaller impact on the degradation of SBS at different depths of SBS MA.

4. Conclusions

This study characterized the high-temperature property, medium-temperature rheological property, adhesion, cohesion, and chemical compositional changes of asphalt binder under aqueous solutions of different pH values. The improved radar chart was utilized to evaluate its comprehensive properties. The layer-by-layer stripping of asphalt binder was studied to elucidate the evolution behavior of properties. According to the above analysis results, the following conclusions can be summarized.

(1) The dissolution and cracking phenomena occur on the microscopic surface of asphalt binders under aqueous solutions of different pH values. The pH 3 solution demonstrates the greatest effect on the morphology of 90 asphalt and SBS MA, resulting in the wide cracks on 90 A and the network cracks on SBS MA. Neutral and alkali solutions have no significant effect on the microscopic morphology of SBS MA.

(2) The improved radar chart illuminates that the pH 3, pH 5, pH 7, pH 9, and pH 11 solutions reduced the f of 90 A by 20.8%, 20.2%, 1.5%, 14.0%, and 25.5%, respectively. For SBS MA, the pH 3, pH 5, pH 7, pH 9, and pH 11 solution decreased the f by 23.2%, 17.7%, 4.6%, 8.7%, and 13.0%, respectively. The acid solutions significantly affect the comprehensive properties of 90 A, but their pH value has little effect. When pH is greater than or equal to 7, 90 A exposure to the higher pH value reveals the worse comprehensive properties. Acid solute and alkali solute can aggravate the effect of aqueous solution on the comprehensive properties of SBS MA, and the degree of aggravation increases with the increase of solute concentration.

(3) Asphalt binder exhibits distinct gradient damage behaviors under different solute environments. The $I_{C=O}$ and $I_{S=O}$ of 90 A at 0–100 μm are easily damaged by aqueous solutions, with the pH 3 solution causing the greatest damage at 25–50 μm. The $I_{C=O}$ and $I_{S=O}$ of 90 A are damaged from the surface to the inner layers by the pH 7 and pH 11 solutions. The $I_{C=O}$, $I_{S=O,}$ and $I_{C=C}$ of SBS MA at 25-50 μm are most reduced by the pH 3 solution, followed by 50-100 μm and 0-25 μm. The $I_{C=O}$, $I_{S=O,}$ and $I_{C=C}$ of SBS MA are initially increased and then decreased back towards the control level in the pH 7 solution, with the most serious damage occurring at 25-100 μm. In the pH 11 solution, the $I_{C=O}$, $I_{S=O,}$ and $I_{C=C}$ are influenced layer by layer, with 0-50 μm being more affected.

The above conclusions have comprehensively assessed the influence law of acid and alkaline environments on the performance of asphalt binder and verified its gradient damage behavior. The findings presented in this study provide a theoretical basis for exploring the damage mechanism of pavement and the application design of asphalt binder. Further research is essential to investigate the performance evolution

behavior across multiple length scales including asphalt mastic, mortar, and mixture.

CRediT authorship contribution statement

Wan Pei: Validation. **Xu Haiqin:** Writing – review & editing. **Xu Shi:** Project administration, Methodology. **Yang Chao:** Writing – review & editing, Methodology. **Zou Yingxue:** Writing – original draft, Investigation, Conceptualization. **Wu Shaopeng:** Supervision, Project administration. **Lu Ziyu:** Investigation. **Amirkhanian Serji:** Visualization, Supervision. **Chen Anqi:** Writing – review & editing, Validation. **Liu Quantao:** Software, Methodology.

Declaration of Competing Interest

The authors declare that they have no known competing financial interests or personal relationships that could have appeared to influence the work reported in this paper.

Data availability

Data will be made available on request.

Acknowledgements

This work is financially supported by the National Natural Science Foundation of China [52375461], the Hubei Science and Technology Innovation Talent and Service Project (International Science and Technology Cooperation) [2022EHB006], Key R&D Program of Guangxi Province [AB21196061], the National Natural Science Foundation of China [52108416], the National Natural Science Foundation of China [52208444], and the Science and Technology Project of the Department of Transportation of Guangxi Autonomous Region [2021-MS5-125].

References

[1] D.M. Mocelin, M.M. Isied, C. Castorena, Influence of reclaimed asphalt pavement (RAP) and recycled asphalt shingle (RAS) binder availability on the composition of asphalt mixtures, J. Clean. Prod. (2023) 139156.
[2] K.M. Nalbandian, M. Carpio, Á. González, Assessment of the sustainability of asphalt pavement maintenance using the microwave heating self-healing technique, J. Clean. Prod. 365 (2022) 132859.
[3] A.D. Hohmann, M.J. Forrester, M. Staver, B.W. Kuehl, N. Hernández, R. Chris Williams, E.W. Cochran, Chemically mediated asphalt rejuvenation via epoxidized vegetable oil derivatives for sustainable pavements, Fuel 355 (2024) 129374.
[4] Y. Ma, S. Wang, M. Zhang, X. Jiang, P. Polaczyk, B. Huang, Weather aging effects on modified asphalt with rubber-polyethylene composites, Sci. Total Environ. 865 (2023) 161089.
[5] C.J. Spreadbury, K.A. Clavier, A.M. Lin, T.G. Townsend, A critical analysis of leaching and environmental risk assessment for reclaimed asphalt pavement management, Sci. Total Environ. 775 (2021) 145741.
[6] P. Cui, S. Wu, Y. Xiao, R. Hu, T. Yang, Environmental performance and functional analysis of chip seals with recycled basic oxygen furnace slag as aggregate, J. Hazard. Mater. 405 (2021) 124441.
[7] J. Xie, J. Chen, L. Hu, S. Wu, Z. Wang, M. Li, C. Yang, Preparation, thermochromic properties and temperature controlling ability of novel pellets in ultra-thin wearing course, Constr. Build. Mater. 389 (2023) 131797.
[8] C. Yang, Z. Huang, S. Wu, J. Xie, Z. Zhao, Y. Zou, Y. Lv, Y. Zhao, F. Wang, L. Zhang, Recycling flue gas desulfurization ash in enhancing the comprehensive moisture susceptibility of asphalt mixtures, J. Clean. Prod. 426 (2023) 139062.
[9] J. Li, J. Yu, S. Wu, J. Xie, The mechanical resistance of asphalt mixture with steel slag to deformation and skid degradation based on laboratory accelerated heavy loading test, Mater. (Basel) 15 (3) (2022).
[10] S. Tian, S. Yang, J. Wang, Q. Li, C. Li, X. Cui, P. Ning, Integrated strategy for efficient simultaneous desulfurization and denitrification of flue gas and high value conversion of sulfur and nitrogen resources, J. Hazard. Mater. 440 (2022) 129827.
[11] Y. Meng, J. Lai, S. Mo, G. Fang, S. Deng, X. Wei, F. Yang, Investigating the deterioration mechanism of adhesion between asphalt and aggregate interface under acid rain erosion, Appl. Surf. Sci. 639 (2023) 158171.
[12] Y. Zhao, Z. Zhang, Z. Li, B. Yang, B. Li, X. Tang, Y. Lai, Comprehensive study on saline-alkali soil amelioration with sediment of irrigation area in northeast China, Arab. J. Chem. 16 (4) (2023) 104608.
[13] M.Y. Jat Baloch, W. Zhang, T. Sultana, M. Akram, B.A.A. Shoumik, M.Z. Khan, M. A. Farooq, Utilization of sewage sludge to manage saline–alkali soil and increase crop production: Is it safe or not?, Environ, Technol. Inno 32 (2023) 103266.
[14] J. Zhu, G. Liu, R. Zhao, X. Ding, H. Fu, ml based approach for inverting penetration depth of SAR signals over large desert areas, Remote Sens. Environ. 295 (2023) 113643.
[15] X. Wang, X. Geng, B. Liu, D. Cai, D. Li, F. Xiao, B. Zhu, T. Hua, R. Lu, F. Liu, Desert ecosystems in China: Past, present, and future, Earth-Sci. Rev. 234 (2022) 104206.
[16] J.B. Zhang, C. Dai, Z. Wang, X. You, Y. Duan, X. Lai, R. Fu, Y. Zhang, M. Maimaitijiang, K.H. Leong, Y. Tu, Z. Li, Resource utilization of rice straw to prepare biochar as peroxymonosulfate activator for naphthalene removal: Performances, mechanisms, environmental impact and applicability in groundwater, Water Res 244 (2023) 120555.
[17] X. Zhang, I. Hoff, H. Chen, Characterization of various bitumen exposed to environmental chemicals, J. Clean. Prod. 337 (2022) 130610.
[18] H. Yang, L. Pang, Y. Zou, Q. Liu, J. Xie, The effect of water solution erosion on rheological, cohesion and adhesion properties of asphalt, Constr. Build. Mater. 246 (2020) 118465.
[19] Y. Zou, S. Amirkhanian, S. Xu, Y. Li, Y. Wang, J. Zhang, Effect of different aqueous solutions on physicochemical properties of asphalt binder, Constr. Build. Mater. 286 (2021) 122810.
[20] L. Pang, X. Zhang, S. Wu, Y. Ye, Y. Li, Influence of water solute exposure on the chemical evolution and rheological properties of asphalt, Materials 11 (6) (2018) 983.
[21] Y. Meng, C. Hu, Y. Tang, D. Großegger, W. Qin, Investigation on the erosion mechanism of simulated salt conditions on bitumen, Constr. Build. Mater. 334 (2022) 127267.
[22] C. Li, F. Ma, Z. Fu, J. Dai, Y. Wen, K. Shi, Investigation of the solution effects on asphalt binder and mastic through molecular dynamics simulations, Constr. Build. Mater. 345 (2022) 128314.
[23] C. Li, W. Qin, Z. Fu, J. Dai, F. Ma, Comparative evaluation on decay process of asphalt-aggregate interfaces under solution erosion, Constr. Build. Mater. 400 (2023) 132698.
[24] Y. Zou, H. Xu, S. Xu, A. Chen, S. Wu, S. Amirkhanian, P. Wan, X. Gao, Investigation of the moisture damage and the erosion depth on asphalt, Constr. Build. Mater. 369 (2023) 130503.
[25] D. Astm, Standard Test Method for Penetration of Bituminous Materials, ASTM International,, USA, 2013.
[26] D. Astm, Standard test method for softening point of bitumen (ring-and-ball apparatus), Annual Book of Standards, 2009.
[27] ASTM, Standard test method for ductility of bituminous materials, 2007.
[28] ASTM, Standard test method for solubility of asphalt materials in trichloroethylene, ASTM International West Conshohocken, 2015.
[29] B. Sengoz, E. Agar, Effect of asphalt film thickness on the moisture sensitivity characteristics of hot-mix asphalt, Build. Environ. 42 (10) (2007) 3621–3628.
[30] S. Dos Santos, M.N. Partl, L.D. Poulikakos, Newly observed effects of water on the microstructures of bitumen surface, Constr. Build. Mater. 71 (2014) 618–627.
[31] C. Yan, W. Huang, Q. Lv, Study on bond properties between RAP aggregates and virgin asphalt using Binder Bond Strength test and Fourier Transform Infrared spectroscopy, Constr. Build. Mater. 124 (2016) 1–10.
[32] A. Ramm, N. Sakib, A. Bhasin, M.C. Downer, Optical characterization of temperature- and composition-dependent microstructure in asphalt binders, J. Microsc. 262 (3) (2015) 216–225, 216.
[33] X. Gong, Q. Liu, H. Wang, P. Wan, S. Chen, J. Wu, S. Wu, Synthesis of environmental-curable CO_2-based polyurethane and its enhancement on properties of asphalt binder, J. Clean. Prod. 384 (2023) 135576.
[34] M. Alae, L. Xu, Z. Cao, X. Xu, F. Xiao, Fatigue and intermediate-temperature cracking performance of rejuvenated recycled asphalt binders and mixtures: A review, J. Clean. Prod. 384 (2023) 135587.
[35] W. Zeiada, H. Liu, H. Ezzat, G.G. Al-Khateeb, B. Shane Underwood, A. Shanableh, M. Samarai, Review of the Superpave performance grading system and recent developments in the performance-based test methods for asphalt binder characterization, Constr. Build. Mater. 319 (2022) 126063.
[36] X. Chen, D. Ren, G. Tian, J. Xu, R. Ali, C. Ai, Investigation on moisture damage resistance of asphalt pavement in salt and acid erosion environments based on Multi-scale analysis, Constr. Build. Mater. 366 (2023) 130177.
[37] C. Yang, S. Wu, P. Cui, S. Amirkhanian, Z. Zhao, F. Wang, L. Zhang, M. Wei, X. Zhou, J. Xie, Performance characterization and enhancement mechanism of recycled asphalt mixtures involving high RAP content and steel slag, J. Clean. Prod. 336 (2022) 130484.
[38] J. Cai, Y. Wen, D. Wang, R. Li, J. Zhang, J. Pei, J. Xie, Investigation on the cohesion and adhesion behavior of high-viscosity asphalt binders by bonding tensile testing apparatus, Constr. Build. Mater. 261 (2020) 120011.
[39] X. Wang, J. Ren, X. Gu, N. Li, Z. Tian, H. Chen, Investigation of the adhesive and cohesive properties of asphalt, mastic, and mortar in porous asphalt mixtures, Constr. Build. Mater. 276 (2021) 122255.
[40] Y. Lv, S. Wu, N. Li, P. Cui, H. Wang, S. Amirkhanian, Z. Zhao, Performance and VOCs emission inhibition of environmentally friendly rubber modified asphalt with UiO-66 MOFs, J. Clean. Prod. 385 (2023) 135633.
[41] C. Yang, S. Wu, J. Xie, S. Amirkhanian, Z. Zhao, H. Xu, F. Wang, L. Zhang, Development of blending model for RAP and virgin asphalt in recycled asphalt mixtures via a micron-Fe3O4, Tracer, J. Clean. Prod. 383 (2023) 135407.
[42] Y. Lv, S. Wu, N. Li, H. Wang, P. Cui, H. Xu, Y. Zhao, C. Yang, X. Zhou, S. Amirkhanian, Environmental hazard reduction and anti-aging enhancement of steel slag powder-asphalt mastic based on TiO2@UiO-67, Compos., J. Clean. Prod. 419 (2023) 138331.
[43] Y. Li, S. Wu, Q. Liu, S. Nie, H. Li, Y. Dai, L. Pang, C. Li, A. Zhang, Field evaluation of LDHs effect on the aging resistance of asphalt concrete after four years of road service, Constr. Build. Mater. 208 (2019) 192–203, 192.

[44] S. Dong, D. Wang, P. Hao, Q. Zhang, J. Bi, W. Chen, Quantitative assessment and mechanism analysis of modification approaches for cold recycled mixtures with asphalt emulsion, J. Clean. Prod. 323 (2021) 129163.
[45] Z. Wang, S. Wu, C. Yang, J. Xie, Y. Xiao, Z. Zhao, F. Wang, L. Zhang, Quantitative assessment of road performance of recycled asphalt mixtures incorporated with steel slag, Materials 15 (14) (2022) 5005.
[46] M. Wu, H. Zhang, Study on rheological properties and damage mechanism of asphalt under acid-alkali precipitation corrosion, Chem. Phys. Lett. 831 (2023) 140853.
[47] W. Pu, C. Shen, X. Tang, B. Wei, N. Zhao, Z. Mei, Research Advances about Oil-water Interfacial Dilational Viscoelasticity in Chemical Flooding, Oilfield Chem. 03 (2018) 562–570.
[48] W. Xiong, Y. Liu, Y. Muhammad, F. Han, L. Yang, X. Jin, Z. Zhao, J. Li, MXene by regulating etching conditions enhanced UV resistance of SBS modified asphalt: Evaluating asphalt photo-oxidation and SBS degradation, Constr. Build. Mater. 377 (2023) 131006.
[49] X. Zhou, T.B. Moghaddam, M. Chen, S. Wu, S. Adhikari, Biochar removes volatile organic compounds generated from asphalt, Sci. Total Environ. 745 (2020) 141096.
[50] L.P. Ingrassia, F. Cardone, F. Canestrari, X. Lu, Experimental investigation on the bond strength between sustainable road bio-binders and aggregate substrates, Mater. Struct. 52 (4) (2019).
[51] K. Shi, F. Ma, Z. Fu, R. Song, D. Yuan, Enhancing aged SBS-modified bitumen performance with unaged bitumen additives, Constr. Build. Mater. 412 (2024) 134768.